

Cavendish-HEP-97/05

May 1997

Revised July 1997

**Single-top production in the tW^\pm channel
and Higgs signals via $H \rightarrow W^+W^-$
at the Large Hadron Collider**

Stefano Moretti¹

*Cavendish Laboratory, University of Cambridge,
Madingley Road, Cambridge, CB3 0HE, United Kingdom.*

Abstract

In a recent study by Dittmar and Dreiner it was shown that with appropriate selection cuts the signature of events containing two charged leptons and missing energy represents the best chance of detecting the Standard Model Higgs scalar in the mass range between 155 and 180 GeV, the primary decay of the Higgs being into pairs of charged gauge bosons. The largest background to this channel is due to irreducible W^+W^-X production. In the present paper we calculate the contribution of events of the type $bg \rightarrow tW^\pm \rightarrow bW^+W^- \rightarrow b\ell^+\ell'^-\nu_\ell\bar{\nu}_{\ell'}$, which have not been considered yet within the new selection strategy. We show that the yield of this background is rather large, at the level of that produced by W^+W^- , $t\bar{t}$ or tbW^\pm events and thus needs to be incorporated in future experimental analyses. However, we find that its inclusion will not spoil the possibilities of Higgs detection in the above mentioned channel at the Large Hadron Collider.

¹E-mail: moretti@hep.phy.cam.ac.uk

1. Introduction and motivations

In a recent paper by Dittmar and Dreiner [1] (see also Ref. [2]) it was pointed out that the signature of events with two charged leptons and missing energy/momentum at the Large Hadron Collider (LHC) represents the best chance of detecting the Standard Model (SM) Higgs boson in the mass range $155 \text{ GeV} \lesssim M_H \lesssim 180 \text{ GeV}$. In Ref. [1], simple selection criteria were outlined, which should allow one to extract the Higgs decay channel $H \rightarrow W^+W^-$ from the non-resonant W^+W^-X production (where X represents possible additional particles in the final state) with a signal-to-background ratio of about one-to-one, thus allowing a $5\div 10\sigma$ detection with only 5 inverse picobarns of integrated luminosity $\mathcal{L} = \int L dt$. The appealing prospect is that this significance can be achieved in less than one year of running of the CERN machine at the initial low luminosity $L = 10^{33} \text{ cm}^{-2} \text{ sec}^{-1}$. Indeed, this is a clear improvement compared to the Higgs search strategy based on the decay mode $H \rightarrow ZZ^* \rightarrow$ four charged leptons, which was the detection channel exploited even in the most recent experimental simulations [3, 4] for the mentioned Higgs mass range. This is evident if one considers that in order to disentangle a 5σ signal in the latter case at least 100 fb^{-1} are required.

The first studies of the $H \rightarrow W^+W^-$ decay mode [5, 6] in the context of Higgs searches at the LHC date back to Ref. [7] and to the 1990 Workshop [8] for a LHC with $\sqrt{s} = 16 \text{ TeV}$. Further analyses were subsequently performed, in Ref. [9]. In various instances, also several signal-to-background studies were carried out (see Section 2 of Ref. [1] for a review). The unanimous conclusion was that the $H \rightarrow W^+W^- \rightarrow \ell^+\ell'^-\nu_\ell\bar{\nu}_{\ell'}$ channel (with $\ell, \ell' = e, \mu$) should provide a useful tool to detect the Higgs boson in the mentioned mass range, though more appropriate analyses (including hadronisation and detector effects) were recognized to be needed to support those (mostly parton level) results.

This was done in Ref. [1], by using the Monte Carlo (MC) program PYTHIA [10]. Further refinements were also introduced there, which were not included in the previous literature. Namely, (i) the inclusion of $W^\pm \rightarrow \tau^\pm\nu_\tau \rightarrow \ell^\pm\nu_\ell\nu_\tau$ decays (with $\ell = e, \mu$); (ii) the simulation of the background due to $gg \rightarrow tbW^\pm$ events [11, 12]; (iii) cuts previously employed [7, 9] were further supported by new constraints, introduced mainly in order to discriminate against the ‘irreducible’ background from continuum production of W^+W^-X events.

It is the purpose of this letter to provide additional material to motivate the exploitation of the $H \rightarrow W^+W^-$ channel in Higgs searches at the LHC, as we have studied the irreducible background due to

$$bg \rightarrow tW^\pm \rightarrow bW^+W^- \rightarrow b\ell^+\ell'^-\nu_\ell\bar{\nu}_{\ell'} \oplus \text{C.C.}, \quad (1)$$

‘single-top’ events via bg -fusion (also called ‘ tW^\pm -production’), which was not considered in Ref. [1], and we will show that this can be reduced to a manageable level by the same selection criteria recommended in [1]. In fact, for completeness, we have also computed the yield of the process

$$bg \rightarrow bW^+W^- \rightarrow b\ell^+\ell'^-\nu_\ell\bar{\nu}_{\ell'} \oplus \text{C.C.}, \quad (2)$$

involving all the tree-level graphs producing the final state $b\ell^+\ell'^-\nu_\ell\bar{\nu}_{\ell'}$: that is, not only

the single-top ones isolated in reaction (1) but also all the other diagrams contributing at the perturbative order $\mathcal{O}(\alpha_{em}^4 \alpha_s)^2$.

With respect to the analysis performed in Ref. [1], we will adopt two simplifications, which we believe will not spoil the validity of our conclusions. First, although we will implement the same cuts considered in Ref. [1], we will confine ourself to the parton level only. However, since at lowest order the final states of reactions (1)–(2) involve only one hadronic system (i.e., the b -quark fragmenting into hadrons) whereas the Higgs signal $H \rightarrow W^+W^- \rightarrow \ell^+\ell'^-\nu_\ell\bar{\nu}_{\ell'}$ is purely leptonic, we expect the effects of hadronisation not to modify drastically the parton level dynamics. Second, we will only discuss the channels $W^+W^- \rightarrow \ell^+\ell'^-\nu_\ell\bar{\nu}_{\ell'}$ with $\ell, \ell' = e, \mu$, thus neglecting the case of W^\pm -decays into tau leptons via the three-body channels $W^\pm \rightarrow \tau^\pm\nu_\tau \rightarrow \ell^\pm\nu_\ell\nu_\tau$. This is done to simplify the description at parton level (especially in the case of the complete process (2)), as in this way we can avoid to calculate complicated two-to-seven and two-to-nine body subprocesses. In practice, contributions involving τ -decays amount to $\approx 1.9\%$ of the total $\approx 7\%$ leptonic branching ratio of W^+W^- -pairs, so that the bulk of the produced W^+W^- events are indeed included in our study. In general, we stress that we are here only interested in the relative rates of signal and background and we expect that the implementation of a full Monte Carlo simulation and the inclusion of the $W^\pm \rightarrow \tau\nu_\tau$ decays will presumably affect both in a rather similar manner.

The reason for studying processes (1)–(2) as a potential background in Higgs searches in the two leptons plus missing energy channel is that single-top production via process (1) has very large event rates at the LHC, as its total cross section amounts to $55 - 60$ pb at $\sqrt{s} = 14$ TeV (see later on), thus being comparable to that of the process $gg \rightarrow tbW^\pm$ considered in Ref. [1] (see, e.g., Ref. [12, 13])³. Furthermore, we stress that compared to the final state tbW^\pm , which eventually yields the signature $b\bar{b}W^+W^-$, that of reaction (1) (and, more generally, of the complete process (2)) can boast only one additional particle with respect to the Higgs signature (this rendering its reduction less effective than that of tbW^\pm events, which have two additional jets⁴). In fact, the latter is produced at lowest order via gluon-gluon fusion into an on-shell Higgs boson, through a top quark loop [14]: $gg \rightarrow H \rightarrow W^+W^- \rightarrow \ell^+\ell'^-\nu_\ell\bar{\nu}_{\ell'}$. However, we notice that the K -factor of Higgs production via gg -fusion has been shown to be very large, around two [15, 16, 17] in the mass range $155 \text{ GeV} \lesssim M_H \lesssim 180 \text{ GeV}$ (and outside, as well [18]). In particular, a large component of the next-to-leading (NLO) order corrections to the gluon-gluon fusion mechanism of Higgs production is due to the real radiation [18] of a quark or gluon, so that also signal events are naturally accompanied by an additional detectable jet inside the detectors.

For reference, we recall that the matrix element of process (1) was already computed

²The symbol \oplus C.C. means that we have calculated also the charged conjugated processes initiated by $\bar{b}g$ -scatterings and these are included in all event rates presented in the following Sections.

³Note that the leading order (LO) rates of the $gg \rightarrow H$ signal for $155 \text{ GeV} \lesssim M_H \lesssim 180 \text{ GeV}$ vary between 10 and 8 picobarns, approximately.

⁴In this respect, we should mention that an extensive compilation and a detailed discussion of processes involving single-top production at hadron colliders has recently been given [12]. In particular, according to the classification of Ref. [12], there are six of these different hard parton scatterings. However, process (1) is the only one contributing at lowest order to the irreducible background W^+W^-X with one additional particle in the final state (i.e., $X \equiv b$), as the others always produce a second (light) jet.

in Ref. [19] and first studied in the context of Higgs searches (and of W^+W^- physics, as well) in Ref. [20] (for its relevance in the case of top-quark physics, see Ref. [12]). However, only the invariant mass region $M_{tW} \equiv \sqrt{\hat{s}} > 850$ GeV was considered there, as a background to signatures of heavy Higgs bosons decaying into longitudinal polarised W^+W^- -pairs [21].

The plan of this paper is as follows. In the next Section we give some details of the calculation. Section 3 is devoted to a discussion of the results. Our conclusions are in Section 4.

2. Calculation

The tree-level Feynman ‘topologies’ that one needs for computing processes (1)–(2) are given in Fig. 1. Once all the internal propagator are correctly inserted one gets a total of 43 Feynman graphs (the single-top diagrams pertaining to reaction (1) can be obtained from the topologies 2 and 3). To calculate the corresponding amplitude squared we have used MadGraph [22] and HELAS [23]. The integrations over the appropriate phase spaces have been performed by using VEGAS [24]. The codes produced have been carefully checked for gauge and BRS [25] invariance. Furthermore, the total cross section for process (1), obtained by selecting the only two graphs with on-shell top production out of those displayed in Fig. 1, has been compared against the results given in Ref. [12] for the Tevatron and in Ref. [20] for the Superconducting Super Collider (SSC), with identical choice of parameters, cuts (where applied) and structure functions, and perfect agreement has been found. The signal rates have been computed by using the program already adopted in Refs. [26, 27]. However, contrary to the case of Ref. [26] where NLO rates were used to calculate the Higgs production cross sections via gg -fusion, and in line with Refs. [1, 27], we have used here the LO results. This has been done for consistency, as one-loop calculations do not exist to date for processes (1) and (2). It is however important to point out that whereas the complete corrections to the main Higgs production process via gluon–gluon fusion are large and positive [18] those to the single-top process (1) are expected to be much smaller [12].

The b -quark in the initial state of reactions (1)–(2) has been treated as a constituent of the proton with the appropriate momentum fraction distribution $f_{b/p}(x, Q^2)$, as given by the parton distribution functions (PDFs). As default set of the latter we have used MRS(A) [28]. However, as the PDFs of the gluon inside the proton are not so well known at medium and small x and since those of b -quarks suffer from potentially large (theoretical) uncertainties (see, e.g., Ref. [29]), we have produced our results in the case of other 4 sets of recent NLO structure functions, which give excellent fits to a wide range of deep inelastic scattering data (including the latest measurements from the HERA ep collider) and to data on other hard scattering processes. These are the packages MRS(A', G, R1, R2) [28, 30, 31]. The QCD strong coupling α_s entering explicitly in the production cross sections and implicitly in the parton distributions has been evaluated using the CERLIB package at the scale $\mu = \sqrt{\hat{s}}$ (i.e., the CM energy at parton level). We will discuss the μ dependence of the LHC rates in the following Section. Indeed, one should remember that also the value of α_s associated with each parton set represents in principle a residual source of error in the predictions

of the different PDFs. However, the value adopted in each set is chosen to match the data during the extraction, so that we do not expect α_s to be a significant source of uncertainty.

In the numerical calculations we have adopted the following values for the electromagnetic coupling constant and the weak mixing angle: $\alpha_{em} = 1/128$ and $\sin^2 \theta_W = 0.2320$. For the gauge boson masses and widths we have taken $M_Z = 91.1888$ GeV, $\Gamma_Z = 2.5$ GeV, $M_{W^\pm} \equiv M_Z \cos \theta_W \approx 80$ GeV and $\Gamma_{W^\pm} = 2.08$ GeV, while for the top mass we have used $m_t = 175$ GeV [32]. All other fermions have been considered massless, including the b -quark. In particular, the choice $m_b = 0$ has been maintained also in the Yukawa couplings of the theory. In this way, no diagram involving radiation of Higgs bosons off the b -lines has been included in process (2). For simplicity, we have set the CKM matrix element of the top-bottom coupling equal to one. In this respect, we recall again Ref. [12], where it was shown that off-diagonal CKM matrix element subprocesses are negligible at the Tevatron. We do expect the same to occur at LHC regimes.

Finally, as total CM energy of the colliding beams at the LHC we have adopted the value $\sqrt{s} = 14$ TeV.

3. Results

Our results are presented in Tab. I and Figs. 2–6. Note that for the time being we assume that no b -tagging identification is exploited in events of the type (1)–(2). The integrated luminosity adopted throughout the paper will be 5 fb^{-1} .

3.1 Selection cuts

As event selection procedure we have adopted the same one exploited in Ref. [1], to which we refer the reader for a detailed discussion concerning the meaning of the various cuts. We only tabulate these here, in order to introduce a notation that will be used in the remainder of this paper (note that the two leptons ℓ and ℓ' must be of opposite sign). Following the same numerical sequence as in [1], we ask (at parton level):

1. $p_T^{\ell, \ell'} > 10$ GeV, p_T^ℓ or $p_T^{\ell'} > 20$ GeV, $\theta_{\ell, \ell'} > 10^\circ$, for the transverse momentum and the separation angle of the two leptons;
2. $|\eta^{\ell, \ell'}| < 2$, for the pseudorapidity of the two leptons;
3. $E_b < 5$ GeV if $\theta_{b\ell, b\ell'} < 20^\circ$, for the energy of the b -quark and the separation angles between the leptons and the b -quark;
4. $M_{\ell\ell'} < 80$ GeV, for the dilepton mass;
5. $p_T^{\text{miss}} > 20$ GeV, for the missing transverse momentum of the event;
6. $\phi < 135^\circ$, for the angle between the two leptons in the plane transverse to the beam direction;

7. if $|\eta^b| < 2.4$ then $p_T^b < 20$ GeV, for the transverse momentum and the pseudorapidity of the b -quark;
8. $|\cos\theta| < 0.8$, for the cosine of the dilepton system with respect to the beam direction;
9. the enforcement $10^\circ < \phi < 45^\circ$, for the same angle defined in 6.;
10. $M > 140$ GeV, for the estimated invariant mass of the W^+W^- -system;
11. $0 < \cos\xi < 0.3$, for the angle between the lepton with the largest transverse momentum, boosted to the dilepton rest frame, and the momentum vector of the dilepton system.

A few comments are in order before proceeding further, concerning the application of cuts 3. and 7. As for cut 3., according to our parton level implementation, background events are rejected if the b -quark is energetic and is found near one of the leptons. On the one hand, we certainly expect the b -quark to be very fast. On the other hand, we do not see a priori any reasons why the quark and the leptons should be created in collinear configurations. This is in fact confirmed by the spectra given in Fig. 2a. However, things would look quite different at hadron level. In fact, the jet produced by the bottom quark would have a finite size and the hadrons produced in the showering would carry only a fraction of the original parton energy. Although we miss these two aspects, we stress that the two systematics errors we introduce with our treatment do work in opposite directions, so to counterbalance each other. Cut 7. will have no effect on our signal rates, as we are considering here neither τ -decay modes nor initial state QCD radiation, whereas for the background it will act directly on the b -parton. This corresponds to an overestimate of the signal, while we believe that the accepted fraction of background events will be predicted accurately, as the efficiency in reconstructing the b -momentum from the hadrons should be rather high because of the clean environment (the two leptons) in which the b -quark fragments. Whichever is the interplay between parton and hadron level, is anyway clear that it is cut 7. that will introduce a strong reduction factor on the background, as the b -jet will be easily detectable in pseudorapidity and will also have a large transverse momentum⁵ (see Fig. 2b).

3.2 Theoretical error

As first step of our analysis we have compared the production rates of process (1) and (2) and found that in Higgs searches (that is, for the selection cuts 1.–11.) the additional contributions from the non-top diagrams of Fig. 1 are negligible. Therefore, in the following we will neglect them.

As one of the possible means of estimating the uncertainty of the theoretical predictions on the gluon distribution (and hence the b -one) we have calculated the cross section for on-shell single-top production via the two-to-two body process $bg \rightarrow tW^\pm \oplus \text{C.C.}$

⁵Note that Fig. 2b has been plotted after having already implemented the constraints 1.–6., and so will be in all forthcoming Figures.

for the mentioned five sets of PDFs. The spread around the value obtained from MRS(A) (the set that we will adopt as a default in the following) is between -9% (from MRS(G)) and $+3\%$ (from MRS(R2)). This will represent throughout the paper the conservative estimate at present time of the uncertainty on the bg -fusion cross section into single-top quarks due to the parton distributions. Note that the above values roughly compare to those identified (for the same sets) in Ref. [26] for the case of gg -fusion into an on-shell Higgs, so that this helps in this context in carrying out a consistent signal-to-background analysis.

Finally, the factorisation scale dependence (which quantifies our ignorance of higher order corrections) of the background rates via process (1) has been estimated by varying μ in the range $\sqrt{\hat{s}}/2 < \mu < 2\sqrt{\hat{s}}$ when calculating the total cross section. We notice that, using MRS(A), differences with respect to the rate at $\mu = \sqrt{\hat{s}}$ are less than 0.1% at $\mu = \sqrt{\hat{s}}/2$ and -3% at $\mu = 2\sqrt{\hat{s}}$. We have verified that similar effects also occur when other PDFs are used. Such numbers are rather small and presumably comparable with the experimental uncertainties⁶.

3.3 Kinematics and event rates

One should expect the impact of the cuts 8. and 9. to be similar on both signal and background, as can be noticed from Figs. 3 and 4, respectively. In fact, the shapes of the corresponding distributions are almost identical⁷.

Not even the invariant mass M of the reconstructed (from the lepton and the missing momenta) W^+W^- -system is helpful to discriminate the signal from the background (see Fig. 5). In fact, the background spectrum is almost entirely beyond the minimum value of 140 GeV implied by cut number 10. The discrimination power of such constraint is thus very limited, if not self-defeating.

The only cut among those introduced in Ref. [1] to reduce the irreducible W^+W^-X background from W^+W^- , $t\bar{t}$ and tbW^\pm events which is also effective against $bg \rightarrow tW^\pm$ is cut 11., as can be appreciated from Fig. 6. In fact, the two charged leptons from the background have a rather large angular spread, so that the maximum of the background distribution is located around the value 0.6.

The accepted event rates, for both signal and background, for a selection of six Higgs masses, are presented in Tab. I ($\sqrt{s} = 14$ TeV and $\mathcal{L} = 5$ fb⁻¹). When comparing the numbers in Tab. I one should bear in mind that the background rates there should be added to those given in Tab. 2 of Ref. [1]. This should however be done after treating all background sources in W^+W^-X events on the same footing (i.e., consistently at parton or, better, hadron level). This is beyond our intentions and capabilities, our aim here is to make the point that background events from process (1) are large compared to the signal, as they vary between 11% and 22% of the Higgs rates, depending on the mass of the scalar. Therefore, their effect in the signal-to-background significance is of the same order as that of any of the three processes $pp \rightarrow W^+W^-$, $pp \rightarrow t\bar{t}$ and $pp \rightarrow tbW^\pm$ studied in Ref. [1], especially considering the fact that our parton

⁶Note that the scale dependence of processes producing the final state $tW^\pm X$ at the Tevatron has been studied in Ref. [12], where variations between -14% and $+20\%$ were quoted, for μ spanning over the range between $\mu = m_t/2$ and $2m_t$.

⁷Please notice the arrow in Fig. 4 to indicate the maximum value of the signal at $\cos\phi \approx 1$.

level analysis overestimate the signal by a factor of two (compare the numbers in our Tab. I to those in Tabs. 1–2 of Ref. [1] in response to the application of cut number 7.), while more accurately predicting the background rates. Finally, one should notice the effectiveness of the selection strategy based on the cuts 1.–11. against events of the type (1), as the overall reduction factor on this background is above 1000 !

4. Summary and conclusions

In this paper, we have studied the yield of process $bg \rightarrow tW^\pm \rightarrow bW^+W^- \rightarrow b\ell^+\ell'^-\nu_\ell\bar{\nu}_{\ell'}$ (where $\ell, \ell' = e, \mu$) as ‘irreducible’ background to the $gg \rightarrow H \rightarrow W^+W^- \rightarrow \ell^+\ell'^-\nu_\ell\bar{\nu}_{\ell'}$ signature of the Standard Model Higgs boson, which has recently been claimed as the most viable channel to detect such a scalar in the mass range $155 \text{ GeV} \lesssim M_H \lesssim 180 \text{ GeV}$ at the Large Hadron Collider. Although we have confined ourselves to the parton level only, we believe we have performed a consistent signal-to-background analysis, exploiting the same event selection procedure advocated in literature. (In particular, the shape of the parton level distributions used to disentangle the signal from the irreducible W^+W^-X noise resembles very closely those previously obtained at hadron level). This has enabled us to assess that non-resonant W^+W^-X events due to single-top production via bg -fusion are rather numerous, and comparable to the rates of any of the reactions $gg, q\bar{q} \rightarrow t\bar{t}$, $gg \rightarrow tbW^\pm$ and $gg, q\bar{q} \rightarrow W^+W^-$, which have in fact been shown to represent the largest components of the total background to the Higgs detection channel in two charged leptons and missing energy/momentum. In contrast, $bg \rightarrow bW^+W^- \rightarrow b\ell^+\ell'^-\nu_\ell\bar{\nu}_{\ell'}$ events not proceeding via single-top diagrams are negligible. Therefore, we think that the production process $bg \rightarrow tW^\pm$ that we have studied should be included in the experimental Monte Carlo simulations which will be used in order to confirm or disprove the existence of the Higgs scalar of the Standard Model in the above mass range at the CERN proton-proton collider. We believe this to be particularly important, as the discussed signature does not allow one to reconstruct the narrow Higgs resonance (because of the neutrinos escaping the detectors). In fact, the presence of the latter will be established by an ‘event counting’ operation over a rather broad region in mass, where the $H \rightarrow W^+W^-$ signal and the $bg \rightarrow tW^\pm$ background have a very similar shape. For the purpose of aiding future analyses, we make available upon request the electronic version of the matrix element for $bg \rightarrow bW^+W^- \rightarrow b\ell^+\ell'^-\nu_\ell\bar{\nu}_{\ell'}$.

However, we would like to conclude this study by stressing that the inclusion of the single-top background in tW^\pm events will certainly not spoil the chances of detecting the Standard Model Higgs in the advocated decay channel, and that the exploitation of the two charged leptons and missing energy signature remains crucial in Higgs searches at hadron colliders.

5. Acknowledgements

We thank Bryan Webber for reading the manuscript and for useful comments and Herbi Dreiner for his assistance with the bibliography of process (1). We are grateful to the UK PPARC for financial support.

References

- [1] M. Dittmar and H. Dreiner, Phys. Rev. **D55**, 167 (1997).
- [2] M. Dittmar and H. Dreiner, Talk given at the Ringberg Workshop ‘The Higgs Puzzle - What can We Learn from LEP2, LHC, NLC, and FMC ?’, Ringberg, Germany, 8-13 December 1996 [hep-ph/9703401].
- [3] CMS Technical Proposal, CERN/LHC/94-43 LHCC/P1 (December 1994).
- [4] ATLAS Technical Proposal, CERN/LHC/94-43 LHCC/P2 (December 1994).
- [5] T.G. Rizzo, Phys. Rev. **D22**, 722 (1980); W.-Y. Keung and W. J. Marciano, Phys. Rev. **D30**, 248 (1984).
- [6] J. Fleischer and F. Jegerlehner, Phys. Rev. **D23**, 2001 (1981); B.A. Kniehl, Nucl. Phys. **B357**, 439 (1991).
- [7] E.W.N. Glover, J. Ohnemus and S. D. Willenbrock, Phys. Rev. **D37**, 3193 (1988).
- [8] Proceedings of the ‘Large Hadron Collider Workshop’, Aachen, 4-9 October 1990, eds. G. Jarlskog and D. Rein, Report CERN 90-10, ECFA 90-133, Geneva, 1990.
- [9] V. Barger, G. Bhattacharya, T. Han and B. A. Kniehl, Phys. Rev. **D43**, 779 (1991).
- [10] T. Sjöstrand, preprint CERN-TH 7112/93; Comp. Phys. Comm. **39**, 347 (1986); T. Sjöstrand and M. Bengtsson, Comp. Phys. Comm. **43**, 43 (1987).
- [11] R.J.N. Phillips, P.M. Zerwas and J. Zunft, in Ref. [8].
- [12] A.P. Heinson, A.S. Belyaev and E.E. Boos, preprint INP-MSU-96-41-448, UCR-96-25, December 1996 [hep-ph/9612424].
- [13] A.P. Heinson, Invited talk at ‘31st Rencontres de Moriond: QCD and High-energy Hadronic Interactions’, Les Arcs, France, 23-30 March 1996 [hep-ex/9605010].
- [14] H. Georgi, S.L. Glashow, M.E. Machacek and D.V. Nanopoulos, Phys. Rev. Lett. **40**, 692 (1978).
- [15] M. Djouadi, M. Spira and P.M. Zerwas, Phys. Lett. **B264**, 440 (1991).
- [16] S. Dawson, Nucl. Phys. **B359**, 283 (1991).
- [17] S. Dawson and R.P. Kauffman, Phys. Rev. **D49**, 2298 (1993).
- [18] A. Djouadi, M. Spira and P.M. Zerwas, Phys. Lett. **B311**, 255 (1993); K. Melnikov and O. Yakovlev, Phys. Lett. **B312**, 179 (1993); M. Spira, Proceedings of the ‘Ringberg Workshop on Electromagnetic Interactions’, Ringberg, Germany, 5-9 February 1995, 203; D. Graudenz, Proceedings of the ‘30th Rencontres de Moriond: QCD and High Energy Hadronic Interactions’, Meribel les Allues, France, 19-25 March 1995, 65; M. Spira, A. Djouadi, D. Graudenz and P.M. Zerwas, Nucl. Phys. **B453**, 17 (1995).

- [19] F. Halzen and C.S. Kim, *Int. J. of Mod. Phys.* **A2**, 1069 (1987).
- [20] G.A. Ladinsky and C.-P. Yuan, *Phys. Rev.* **D43**, 789 (1991).
- [21] M. Duncan, G.L. Kane and W. Repko, *Nucl. Phys.* **B272**, 517 (1986); G.L. Kane and C.-P. Yuan, *Phys. Rev.* **D40**, 2231 (1989).
- [22] T. Stelzer and W.F. Long, *Comp. Phys. Comm.* **81**, 357 (1994).
- [23] H. Murayama, I. Watanabe and K. Hagiwara, HELAS: HELicity Amplitude Subroutines for Feynman Diagram Evaluations, KEK Report 91-11, January 1992.
- [24] G.P. Lepage, *Jour. Comp. Phys.* **27**, 192 (1978).
- [25] C. Becchi, A. Rouet and R. Stora, *Ann. Phys.* **98**, 287 (1976); G.J. Gounaris, R. Kogerler and H. Neufeld, *Phys. Rev.* **D34**, 3257 (1986).
- [26] Z. Kunszt, S. Moretti and W.J. Stirling, *Z. Phys.* **C74**, 479 (1997).
- [27] S. Moretti, preprint DFTT 79/95, Cavendish-HEP-95/18, DTP/95/104, November 1996 [hep-ph/9612310].
- [28] A.D. Martin, R.G. Roberts and W.J. Stirling, *Phys. Rev.* **D50**, 6734 (1994).
- [29] A.D. Martin, R.G. Roberts, M.G. Ryskin and W.J. Stirling, preprint DTP/96/102, December 1996 [hep-ph/9612449].
- [30] A.D. Martin, R.G. Roberts and W.J. Stirling, *Phys. Lett.* **B354**, 155 (1995).
- [31] A.D. Martin, R.G. Roberts and W.J. Stirling, *Phys. Lett.* **B387**, 419 (1996).
- [32] P. Grannis, plenary talk given at the International Conference on High Energy Physics, Warsaw, 1996.

Table Captions

- [1] The expected signal and background number of events for 5 fb^{-1} at the LHC after the application of the selection criteria discussed in the text. Only the two-body decays $W^\pm \rightarrow \ell\nu_\ell$ with $\ell = e, \mu$ are considered in both signal and background. The parton distribution functions used are MRS(A).

Figure Captions

- [1] Feynman diagram topologies contributing at tree-level to the process $bg \rightarrow b\ell^-\ell'^+\bar{\nu}_\ell\nu_{\ell'}$, where ℓ represents a lepton. Internal wavy lines represent a photon, a Z or a W^\pm , whereas the internal solid ones refer to a lepton, a neutrino, a bottom- or a top-quark, as appropriate. The total number of graph is 43 (excluding Higgs couplings). The single-top diagrams are number 2 and 3. Charge conjugated diagrams can be trivially obtained by reversing the fermion lines.
- [2] Differential distributions in **(a)** energy of the final state b -jet (left plot) and its angular separation from the two leptons (right plot: from that generated by the top-decay W^\pm , solid line, and from that generated by the non-top-decay W^\pm , dashed line) and **(b)** transverse momentum (left plot) and pseudorapidity (right plot) of the final state b -jet in events of the type $bg \rightarrow tW^\pm \rightarrow bW^+W^- \rightarrow b(\ell^-\bar{\nu}_\ell)(\ell'^+\nu_{\ell'})$, with $\ell, \ell' = e, \mu$, at the LHC, **(a)** before the acceptance cuts and **(b)** after the acceptance cuts 1–6. The parton distribution functions used are MRS(A).
- [3] Differential distributions in the polar angle of the dilepton system with respect to the beam direction for the Higgs signal ($M_H = 170 \text{ GeV}$, solid histogram) and the single-top background (dashed histogram) at the LHC after the acceptance cuts 1–6. The parton distribution functions used are MRS(A). Note that the background rates have been divided by two in order to facilitate the comparison between the two curves.
- [4] Differential distributions in the azimuthal angle of the dilepton system in the plane transverse to the beam direction for the Higgs signal ($M_H = 170 \text{ GeV}$, solid histogram) and the single-top background (dashed histogram) at the LHC after the acceptance cuts 1–6. The parton distribution functions used are MRS(A). Note that the background rates have been divided by two in order to facilitate the comparison between the two curves.
- [5] Differential distributions in the estimated invariant mass of the $\ell^-\ell'^+\bar{\nu}_\ell\nu_{\ell'}$ system for the Higgs signal ($M_H = 170 \text{ GeV}$, solid histogram) and the single-top background (dashed histogram) at the LHC after the acceptance cuts 1–6. The parton distribution functions used are MRS(A). Note that the background rates have been divided by two in order to facilitate the comparison between the two curves.
- [6] Differential distributions in the angle between the lepton with highest transverse momentum, boosted to the dilepton rest frame, and the momentum vector of the

dilepton system itself for the Higgs signal ($M_H = 170$ GeV, solid histogram) and the single-top background (dashed histogram) at the LHC after the acceptance cuts 1–6. The parton distribution functions used are MRS(A). Note that the background rates have been divided by two in order to facilitate the comparison between the two curves.

Accepted event rates							
process $pp \rightarrow X$	N_{ev}						
	No cut	cut 1-3	cut 4-6	cut 7	cut 8-9	cut 10	cut 11
$gg \rightarrow H \rightarrow W^+W^-$							
$M_H = 155$ GeV	1832	1032	893	893	209	147	70
$M_H = 160$ GeV	2002	1154	1035	1035	267	208	109
$M_H = 165$ GeV	2017	1179	1054	1054	270	219	119
$M_H = 170$ GeV	1929	1141	988	988	244	199	99
$M_H = 175$ GeV	1829	1087	901	901	215	176	79
$M_H = 180$ GeV	1702	1019	801	801	184	152	61
$bg \rightarrow tW^\pm \rightarrow bW^+W^-$	13408	8254	2794	238	44	42	13
$\sqrt{s} = 14$ TeV $\mathcal{L} = 5$ fb $^{-1}$ $m_t = 175$ GeV							

Tab. I

Diagrams by MadGraph

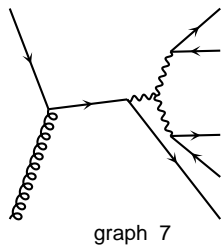
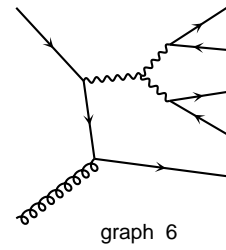
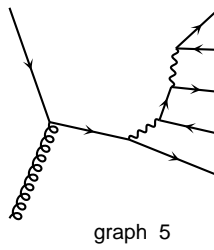
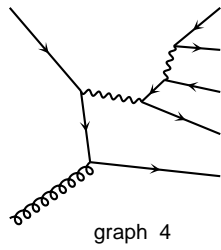
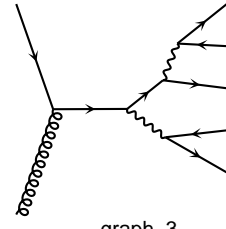
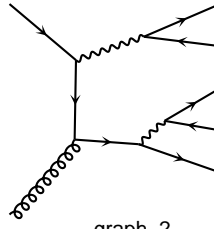
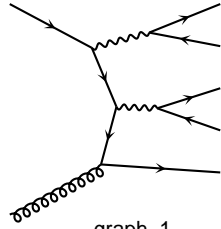


Fig. 1

bg fusion at the LHC, MRS(A)

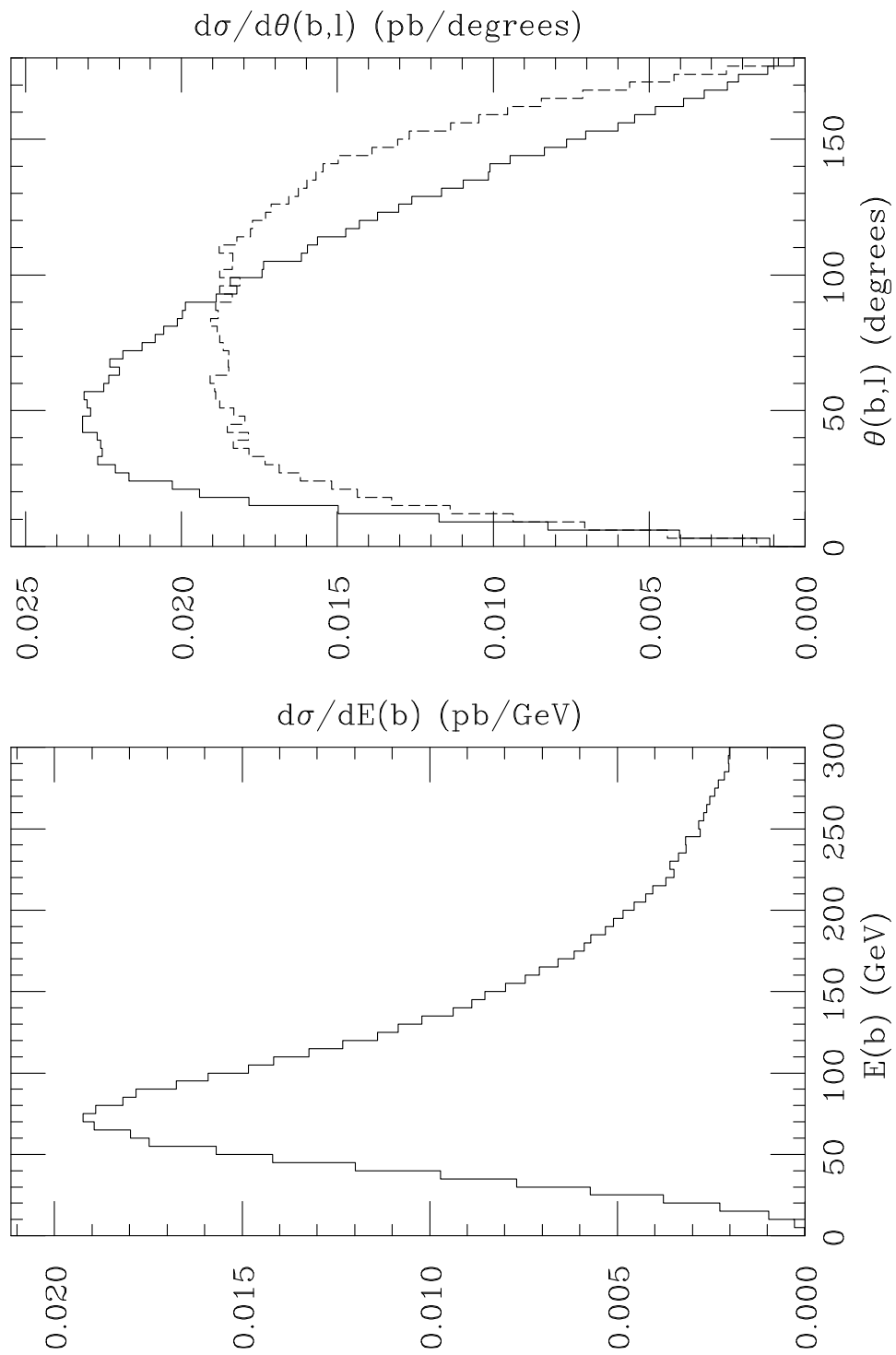


Fig. 2a

bg fusion at the LHC, MRS(A)

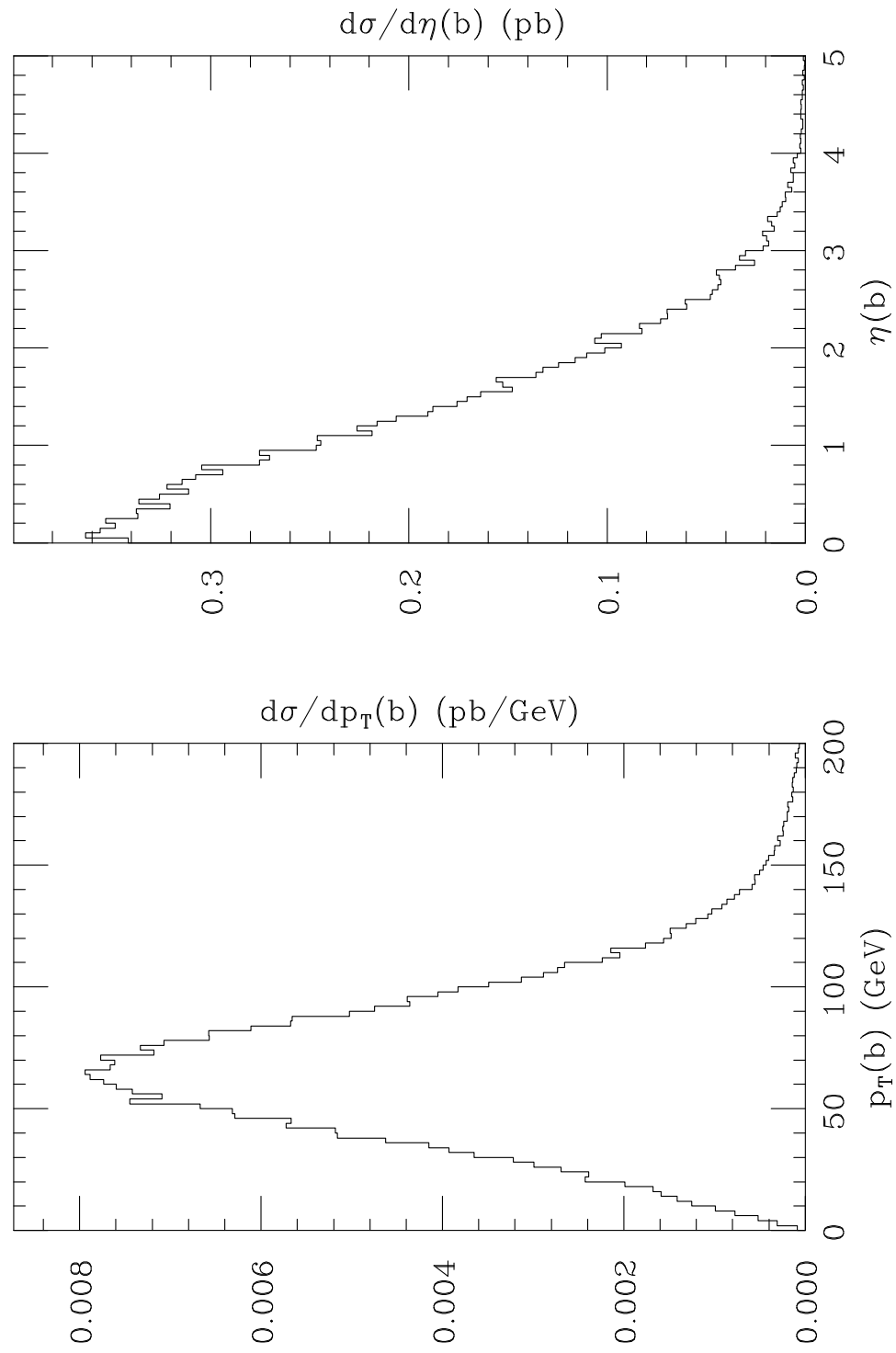


Fig. 2b

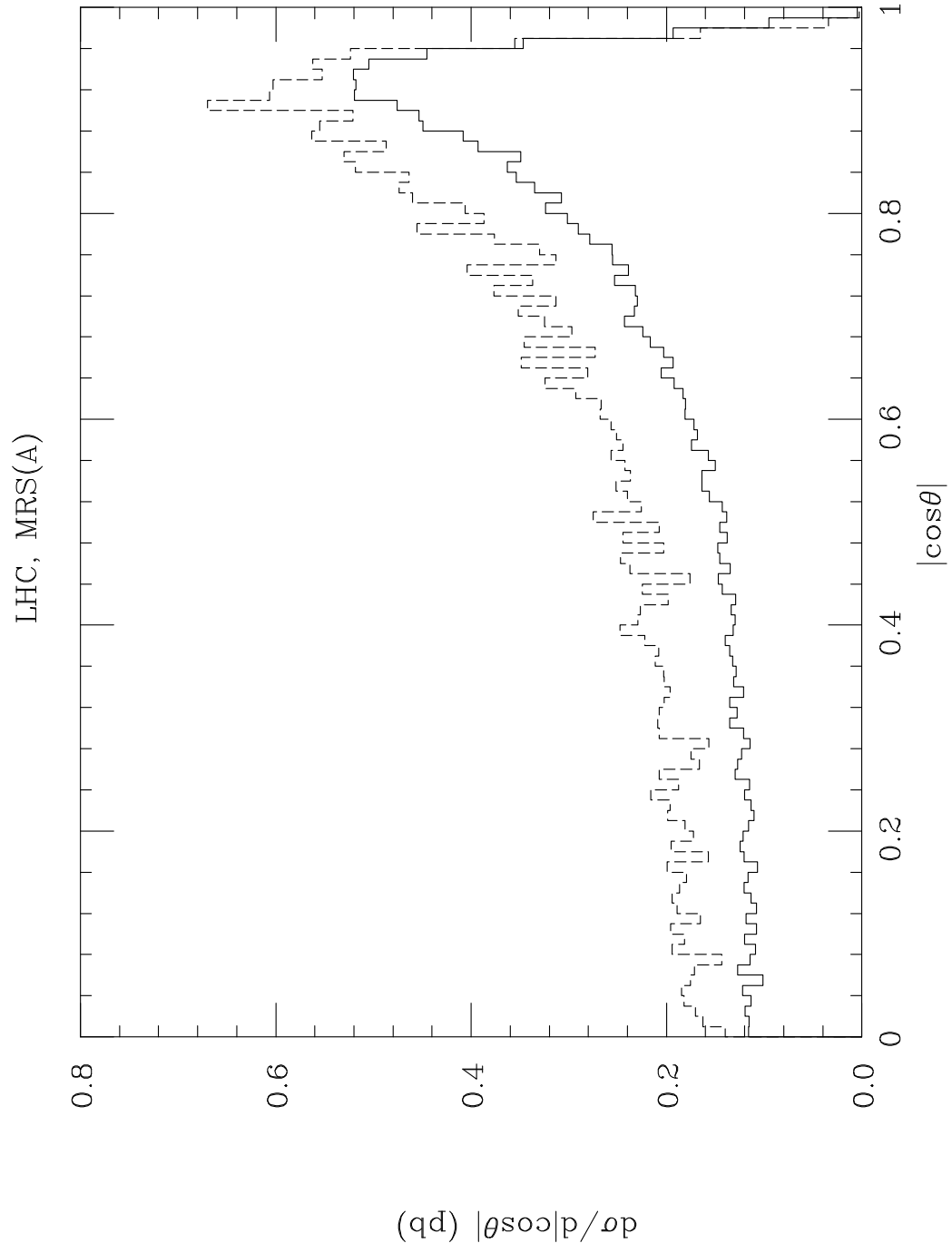


Fig. 3

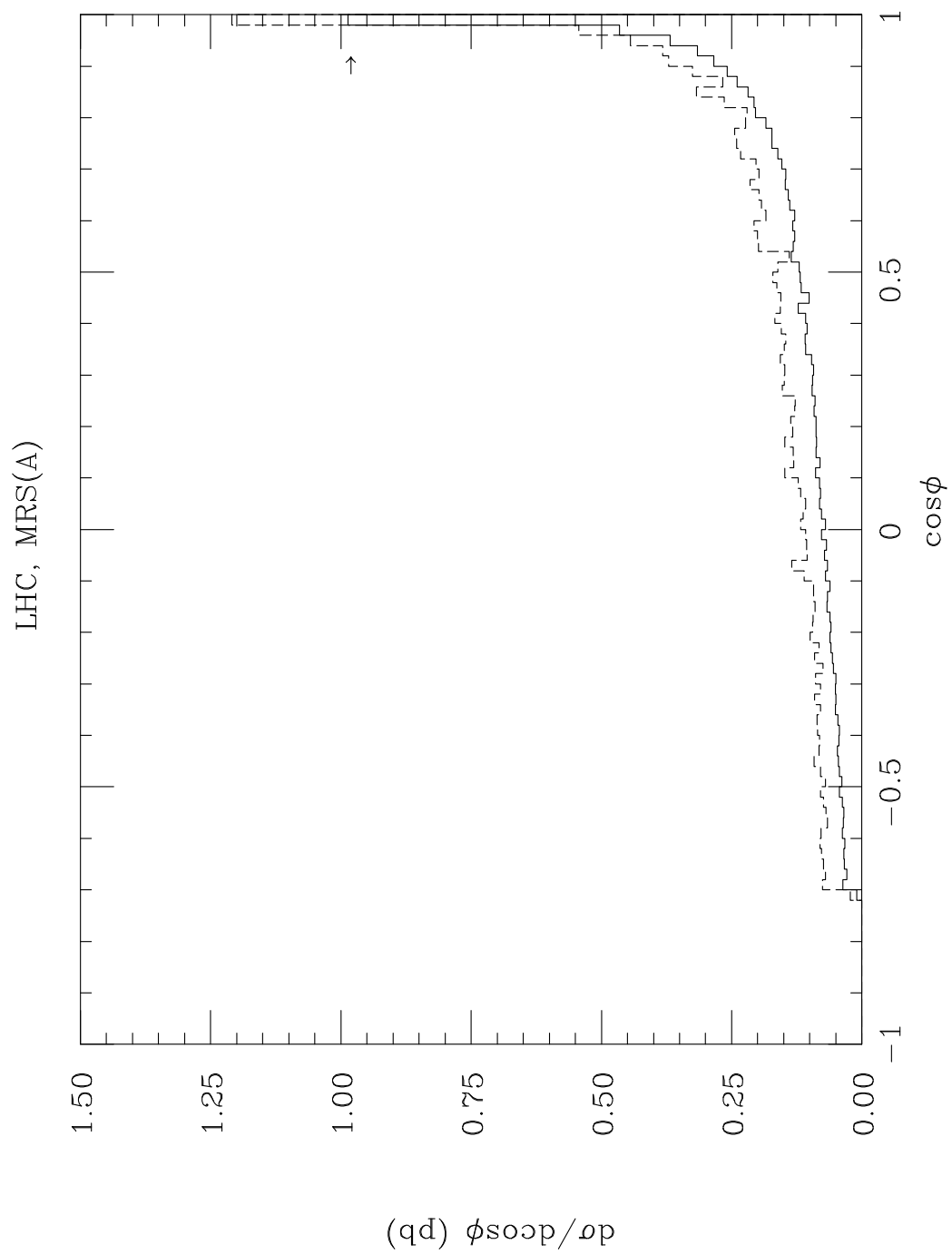


Fig. 4

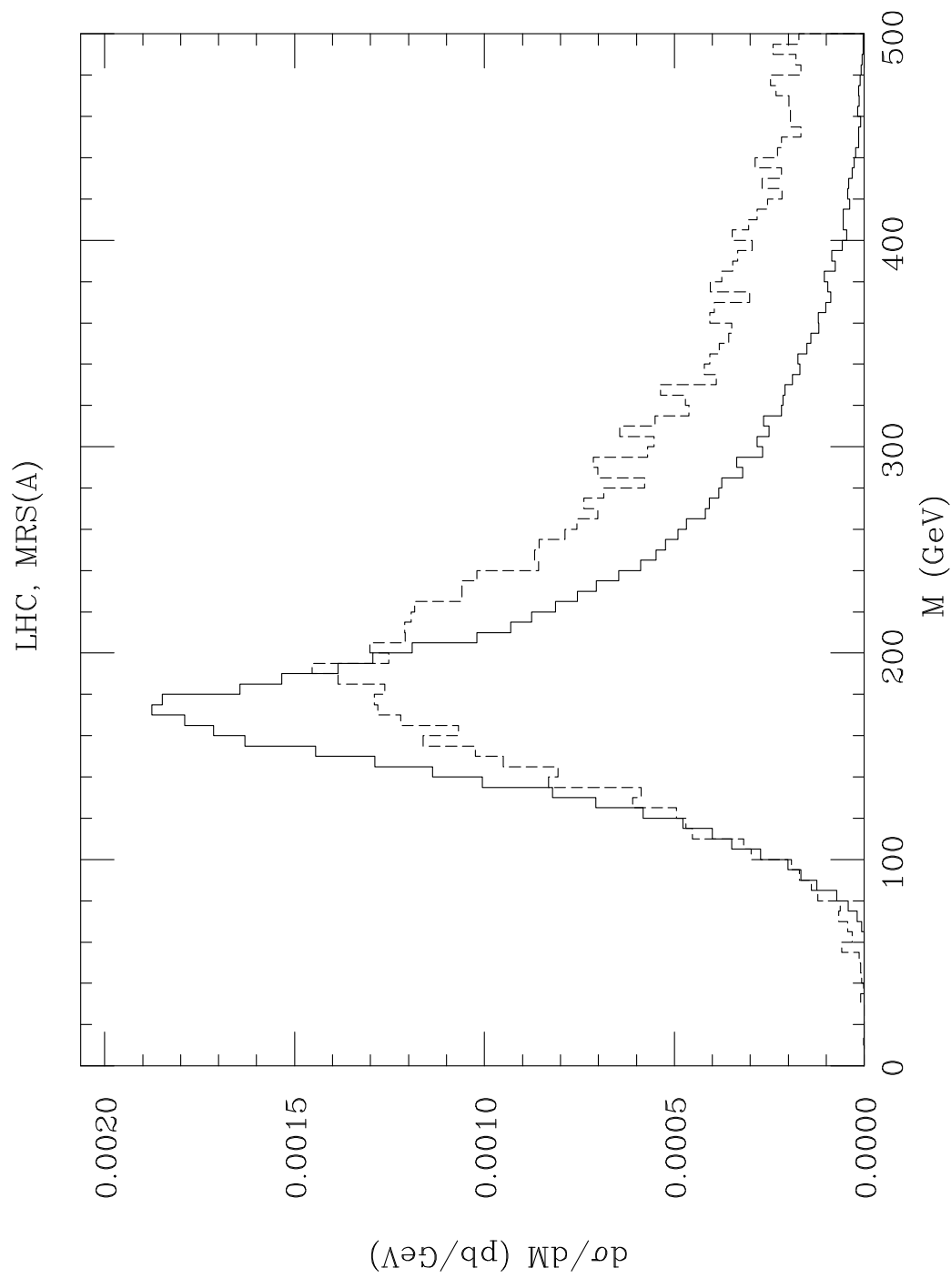


Fig. 5

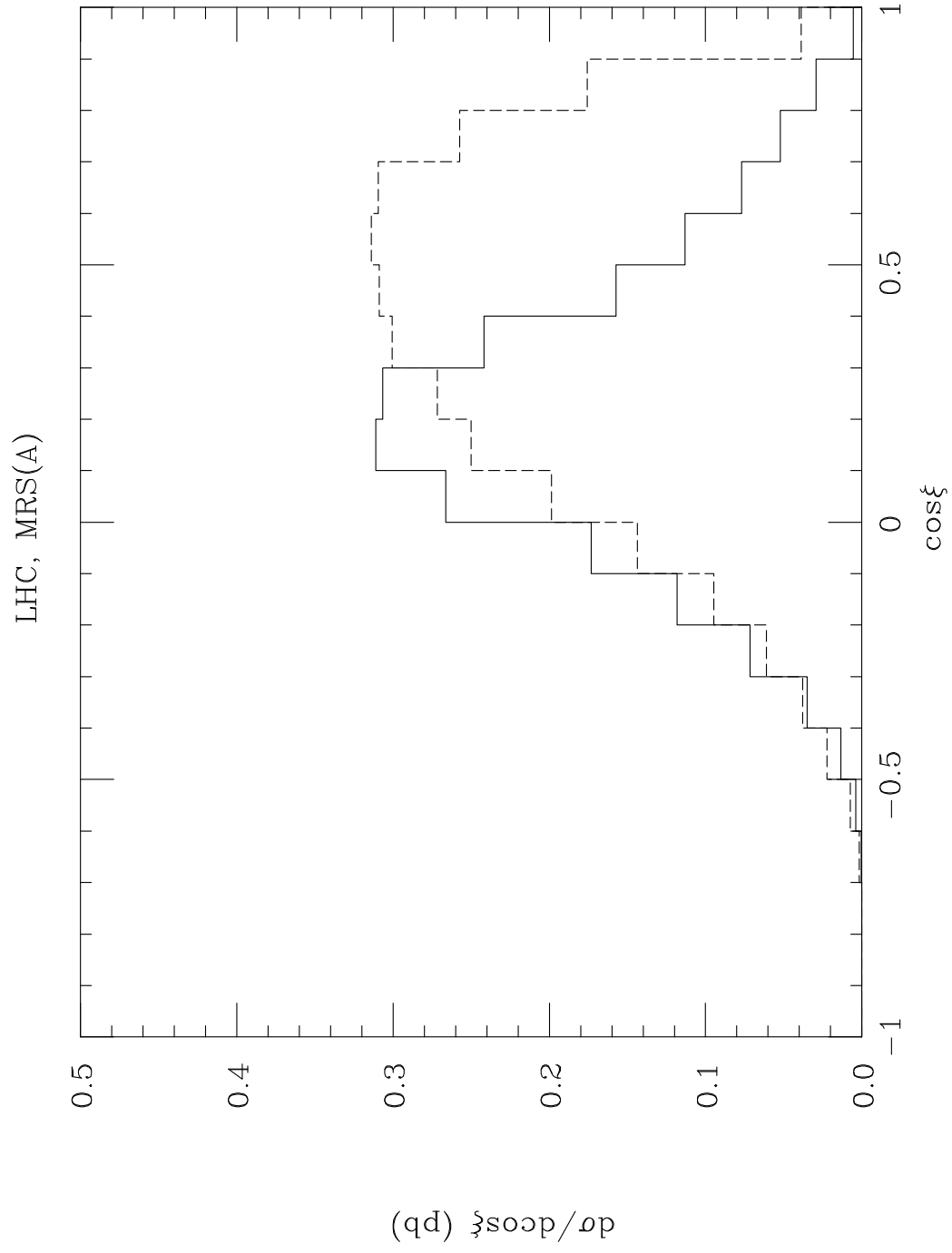


Fig. 6